LiSAD: A Label-efficient Implicit Model with Spatially Adaptive Directional Total Variation for Spatial Transcriptomics

Yinghao Xia[1*], Xiaoxuan Ji[2*], Haoyang Liu[1], Fei Guo[1,3✉], Xikang Feng[1], Liang He[1], Hui Cui[4], Shuang Xu[2], Ran Su[5], Leyi Wei[6], and Qiangguo Jin[1✉]

[1] School of Software, Northwestern Polytechnical University, Shaanxi, China
qgking@nwpu.edu.cn
[2] School of Mathematics and Statistics, Northwestern Polytechnical University, Shaanxi, China
[3] School of Information Technology, Suzhou Institute of Trade and Commerce, Jiangsu, China
[4] Department of Computer Science and Information Technology, La Trobe University, Melbourne, Australia
[5] School of Computer Software, Tianjin University, Tianjin, China
[6] Faculty of Applied Science, Macao Polytechnic University, Macao SAR, China

Abstract. Spatial transcriptomics (ST) provides unprecedented opportunities to understand tissue structures. Spatial domain identification serves as a core task to partition tissue regions. Current methods achieve initial success on such task, however struggle to identify accurate domain boundaries and rarely attempts supervised paradigm. To address these challenges, we propose a **L**abel-efficient **i**mplicit model with **S**patially **A**daptive **D**irectional total variation (LiSAD). LiSAD adopts implicit neural representations (INRs) with a hypergraph learning framework to transform discrete ST data into continuous representations while modeling high-order topological relationships for spots. We propose a spatially adaptive directional total variation (SADTV) regularization for accurate boundary identification. Furthermore, we propose a label-efficient optimization strategy that leverages minimal expert prior knowledge to learn refined biological representations. Experimental results on multiple datasets show that LiSAD outperforms current methods by 3-7% in adjusted rand index (ARI), validating its effectiveness. We propose a practical label-efficient paradigm for ST analysis. LiSAD achieves a superior trade-off between annotation economy and diagnostic accuracy, enabling accurate domain identification with minimal expert priors. Code is available at https://github.com/BioMedIA-repo/LiSAD.

Keywords: Spatial transcriptomics · Continuous representation · Directional total variation · Label-efficient learning.

[*] Y. Xia and X. Ji: Contributed equally to this work. ✉ F. Guo and Q. Jin are co-corresponding authors.

1 Introduction

Spatial transcriptomics (ST) is a technology that aims to decipher cellular interactions and anatomical tissue structures. ST data typically consist of spatial coordinates and their corresponding gene expressions. Current ST technologies are categorized into imaging-based (e.g., STARmap [22]) and sequencing-based (e.g., Visium [20]) methods. Due to its ability to precisely map gene expression within tissue contexts, ST analysis gains widespread attention and emerges as a rapidly evolving field in biology and bioinformatics.

Spatial domain identification is a core task in ST analysis [3]. It aims to partition tissues into functional regions based on gene expression and spatial coordinates, providing a foundation for downstream tasks. Early studies typically apply non-spatial clustering algorithms directly to gene expressions, such as Louvain [21] or K-means [8]. By ignoring spatial structure, these methods fail to align with actual tissue anatomy, yielding discontinuous and fragmented patches. Therefore, researchers propose methods that integrate spatial information. For instance, BayesSpace [28] employs spatial prior to encourage neighboring spots to belong to the same cluster. While these methods improve spatial continuity [15, 28], they rely on predefined spatial adjacency such as a fixed number of neighbors, yielding misleading results in highly heterogeneous tissues.

To overcome the limitations of rigid spatial priors, current research turns to graph neural networks (GNNs) [10, 27, 24, 23], which offer a more flexible framework to model spatial dependencies. SpaGCN [9] first models ST data as graphs, using GNNs to learn node embeddings that integrate gene expression and spatial information. Subsequently, STAGATE [4] introduces a graph attention auto-encoder to adaptively learn importance weights for neighboring nodes. Latest studies, such as STAIG [26], further incorporate contrastive learning to integrate multimodal data, including gene, spatial, and histological information.

Despite the success of current methods, several challenges remain. First, constrained by current technologies, ST data is typically sampled on a discrete spatial grid. Most existing methods model the discrete data directly, failing to construct a continuous spatial field, making it difficult to capture subtle spatial variations. Second, tissues typically exhibit blurred transitions rather than sharp edges, increasing the difficulty of accurate boundary identification [1]. Third, although fully supervised annotation is challenging, pathologists can readily annotate representative spots as expert priors. However, current methods rarely leverage this expert knowledge, defaulting to unsupervised strategies while neglecting the potential of supervised paradigm [16, 7].

To address these challenges, we propose LiSAD, a **L**abel-efficient **i**mplicit model with **S**patially **A**daptive **D**irectional total variation. We adopt implicit neural representations (INRs) [19] to bridge the gap between discrete data and continuous spatial modeling [12]. To accurately identify domain boundaries, we propose a novel spatially adaptive directional total variation (SADTV) regularization to preserve high-frequency spatial details. Moreover, we explore label-efficient learning, utilizing minimal expert prior to improve the performance and clinical utility. Our contributions are as follows:

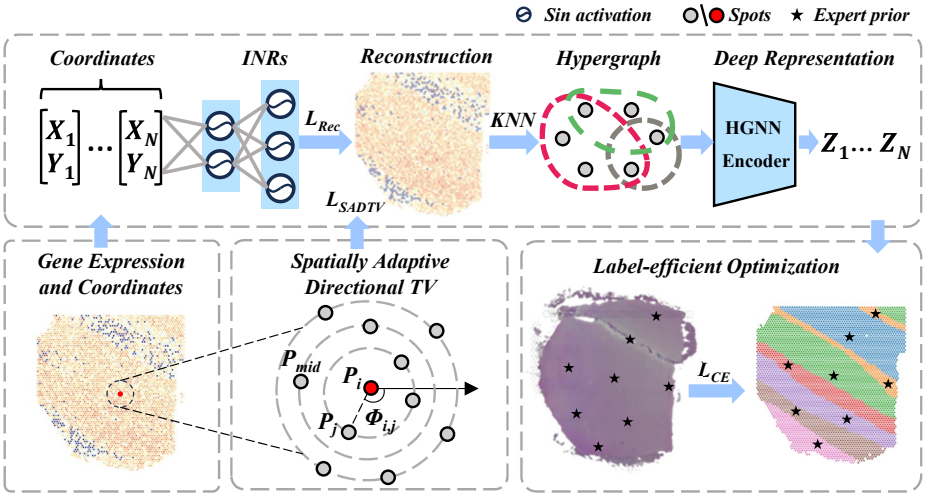

Fig. 1. Overview of our LiSAD. LiSAD utilizes INRs for gene expression reconstruction, a hypergraph encoder to extract deep representations and minimal expert priors to guide the spatial domain identification. The SADTV regularization is proposed to enhance boundary precision.

(1) We propose a representation learning module that fuses INRs with hypergraphs, transforming discrete ST data into a continuous representation and modeling intercellular interactions.
(2) We propose the SADTV, a novel total variation regularization. It adaptively captures the degree of local spatial variation to facilitate accurate domain boundary identification.
(3) We introduce label-efficient learning to spatial domain identification. Through experiments across multiple datasets and models, we demonstrate that label-efficient learning significantly improves accuracy, providing a novel direction for spatial transcriptomics.

2 Method

Figure 1 illustrates the overall pipeline of LiSAD, a label-efficient supervised framework including an implicit neural network, a hypergraph encoder and SADTV regularization.

2.1 INR-enhanced Hypergraph Representation

To address the limitations of discrete sampling in ST data, we leverage INRs to learn a continuous spatial representation [13]. Specifically, the model takes spatial coordinates $P \in \mathbb{R}^{N\times 2}$ as input to reconstruct the gene expression $X_{\text{Rec}} \in$

$\mathbb{R}^{N\times D}$ using a multi-layer perceptron (MLP) with sinusoidal activation functions. The process constructs the continuous function $f_\theta(\cdot) : \mathbb{R}^{N\times 2} \to \mathbb{R}^{N\times D}$, and:

$$X_{\text{Rec}} = f_\theta(P), \quad \mathcal{L}_{\text{Rec}} = ||X_{\text{Rec}} - X||_F^2, \tag{1}$$

where θ is the learnable parameters, $X \in \mathbb{R}^{N\times D}$ is observed gene expression, N is the number of sampling spots, D is the gene expression dimension, and $\mathcal{L}_{\text{Rec}}$ is the reconstruction loss. Moreover, the INR imposes lipschitz continuity [11] for any spatial coordinates p_i and p_j:

$$||f_\theta(p_i) - f_\theta(p_j)||_2^2 \leq L||p_i - p_j||_2^2, \tag{2}$$

where L is the lipschitz constant. This constraint on the rate of change effectively filters out high frequency noise caused by dropouts in data.

In order to extract robust representations from the reconstructed continuous fields, we utilize hypergraphs neural network to model high-order topological relationships [5]. First, X_{Rec} is mapped to a low-dimensional representation $Y \in \mathbb{R}^{N\times d}$ through a linear layer. Meanwhile, based on spatial distance, we utilize the K-nearest neighbors (KNN) algorithm to construct the incidence matrix $H \in \mathbb{R}^{N\times N}$, yielding the hypergraph $\mathcal{G} = (V, E)$. Here, V is the set of nodes and E is the set of hyperedges. Finally, the $\mathcal{G}$ is fed into two stacked hypergraph convolutional layers to extract the deep representation Z:

$$Z = \text{HGNNConv}_2(\sigma(\text{HGNNConv}_1(Y, H)), H), \tag{3}$$

where σ is the ReLU activation function. The hypergraph convolution operator [6] is defined as:

$$\text{HGNNConv}(Y^{(l)}, H) = D_{\text{v}}^{-1} H D_{\text{e}}^{-1} H^T Y^{(l)} \omega^{(l)}, \tag{4}$$

where $D_{\text{v}} \in \mathbb{R}^{N\times N}$ and $D_{\text{e}} \in \mathbb{R}^{N\times N}$ are the diagonal matrices of node degrees and hyperedge degrees, respectively. $\omega^{(l)} \in \mathbb{R}^{d_{\text{in}}\times d_{\text{out}}}$ is the learnable parameters of the l-th layer, where d_{in} and d_{out} are the input and output feature dimensions, respectively. Compared to a simple graph that only describes pairwise relationships, hyperedges can connect any number of nodes [25]. This high-order topology makes them compatible for modeling cellular communities.

2.2 Spatially Adaptive Directional Total Variation

For accurate identification of spatial domain boundaries, we propose the SADTV. It captures fine-grained spatial heterogeneity by modeling local directional variations [18]. Firstly, for spot p_i, we select its $2k$ nearest neighbors to form a set N_i. Then, we design distance-based adaptive Gaussian weights $\Gamma_{i,j}$, ensuring that closer spots contribute more to the local variation:

$$\Gamma_{i,j} = \frac{\exp\left(-\frac{||p_j - p_i||_2^2}{\sigma_i^2}\right)}{\sum_{p_m \in N_i} \exp\left(-\frac{||p_m - p_i||_2^2}{\sigma_i^2}\right)}, \tag{5}$$

where $\sigma_i = \|p_i - p_{\text{mid}}\|_2$ is the distance between p_i and p_{mid}, serving as an adaptive scaling factor. p_{mid} is the neighbor whose distance to p_i is the median of all neighbor. Next, a local polar coordinate system is established with p_i as the origin. For any neighbor $p_j \in N_i$, its azimuthal angle relative to p_i is denoted as $\phi_{i,j}$. We define the local directional variation vector G_i of p_i as the directionally weighted sum of gene expression variations within the neighborhood:

$$G_i = \left\| \sum_{p_j \in N_i} \Gamma_{i,j} \cdot (f_\theta(p_j) - f_\theta(p_i)) \cdot e^{i\phi_{i,j}} \right\|_1, \tag{6}$$

where $e^{i\phi_{i,j}}$ is the spatial direction vector of p_j relative to p_i. G_i effectively aggregates signal variations from different directions within the neighborhood, and its value reflects the intensity of local variations besides p_i. Finally, we utilize the $\mathcal{L}_1$ norm as a regularization term to constrain the INR reconstruction process, defining the SADTV loss function as:

$$\mathcal{L}_{\text{SADTV}} = \sum_{i=1}^{N} G_i. \tag{7}$$

Because of the sparsity-inducing property of the $\mathcal{L}_1$ norm, SADTV ensures high smoothness within the same spatial domain, while preserving and enhancing significant differences in gene expression at domain boundaries.

The computational cost of SADTV is linear with respect to the number of spots and neighbors $O(N \cdot K)$. Since the adaptive Gaussian weights $\Gamma_{i,j}$ and spatial direction vectors $e^{i\phi_{i,j}}$ are precomputed, the additional overhead during training is minimal.

2.3 Label-efficient Optimization

In clinical practice, although full annotation of ST data is costly, pathologists can efficiently annotate a small number of representative spots with high diagnostic certainty. LiSAD aligns with this interactive clinical paradigm through a label-efficient optimization framework. Specifically, $D = \{(p_i, y_i)\}_{i=1}^{M \times S}$ is the annotated dataset, where $y_i \in \{1, \ldots, S\}$ is the corresponding expert labels, S is the number of spatial domains and M is the number of labels selected for each domain. Rather than randomly sampling, M spots are selected from regions with high local label consistency in each domain. To verify the model's robustness, these spots are spatially dispersed within these regions. This strategy effectively simulates the process where experts provide labels in the most confident areas. Then, we feed the deep representation Z extracted in Section 2.1 into a single-layer linear classification head. The model is optimized by minimizing the cross-entropy loss:

$$\mathcal{L}_{\text{CE}} = -\frac{1}{|D|} \sum_{i \in D} \log(\widehat{y}_{i,y_i}), \tag{8}$$

where $\widehat{y}_{i,y_i}$ is the probability value of the i-th spot for the true category y_i. Due to the message-passing mechanism of hypergraph convolutions [6], the label information propagates to all spots. Such optimization allows the sparse supervision signal to guide other spots, achieving precise spatial domain identification.

2.4 Loss Function

In summary, the training of LiSAD is a multi-task joint optimization process. We integrate the reconstruction loss, the SADTV regularization, and the classification loss to obtain the final loss function of the model:

$$\mathcal{L}_{\text{total}} = \mathcal{L}_{\text{CE}} + \mathcal{L}_{\text{Rec}} + \lambda \mathcal{L}_{\text{SADTV}}, \tag{9}$$

where λ is the scale factor of the SADTV regularization.

3 Experiments

3.1 Experimental Setup

Datasets. We evaluate LiSAD on three datasets from different platforms: (1) Human dorsolateral prefrontal cortex (DLPFC) [14], containing 12 slices with manual annotations. (2) Human breast cancer (HBC) [17], a slice exhibits complex tumor microenvironments and heterogeneous cell distribution. (3) Mouse visual cortex (STARmap) [22], an imaging-based dataset with single-cell resolution, used to test the model's performance on high-precision spatial data.
Baselines and Metrics. We compare LiSAD with four recent methods: SpaGCN [9], GraphST[10], SEDR [24], and STAIG [26]. Each baseline is implemented in two modes, default unsupervised mode and label-efficient mode, where a linear classifier is trained using the same labels as LiSAD. Performance is quantified via adjusted rand index (ARI) and normalized mutual information (NMI).
Implementation Details. The INR hidden dimension is set to 30, while the HGNN hidden and embedding layers are 128 and 64, respectively. Hypergraphs are constructed with $K = 10$ neighbors. The M is set to 5. The TV loss weight λ is set to 0.01. The experiments are conducted on an NVIDIA RTX 4090 (24GB) GPU using the Adam optimizer with a learning rate of 0.002 for 300 epochs.

3.2 Performance Comparison

Comparison with Unsupervised Mode. Table 1 shows that LiSAD significantly outperforms all unsupervised methods across three datasets. Notably, on the high-resolution STARmap dataset, LiSAD achieves an ARI of 0.80, a 22% improvement over the best unsupervised baseline STAIG. The above results confirm LiSAD's consistent advantage in spatial domain identification.
Comparison with Label-efficient Mode. Table 1 shows that LiSAD maintains a clear lead in label-efficient mode. For instance, in the DLPFC dataset, LiSAD reaches 0.76 ARI, surpassing the second-best STAIG by 6%. Besides,

Table 1. Quantitative performance comparison (ARI, NMI). The best results are **bolded** and the second best are underlined.

Method	Mode	DLPFC		HBC		STARmap	
		ARI↑	NMI↑	ARI↑	NMI↑	ARI↑	NMI↑
SpaGCN	Unsupervised	0.45	0.58	0.53	0.66	0.26	0.29
GraphST	Unsupervised	0.57	0.67	0.55	0.66	0.36	0.46
SEDR	Unsupervised	0.50	0.66	0.37	0.64	0.58	0.68
STAIG	Unsupervised	0.61	0.67	0.57	0.69	0.52	0.65
SpaGCN	Label-efficient	0.61	0.64	0.67	0.68	0.35	0.39
GraphST	Label-efficient	0.51	0.58	0.64	0.65	0.50	0.59
SEDR	Label-efficient	0.64	0.69	0.63	0.66	0.52	0.59
STAIG	Label-efficient	0.70	0.70	0.66	0.73	0.73	0.79
LiSAD	Label-efficient	**0.76**	**0.76**	**0.69**	**0.74**	**0.80**	**0.84**

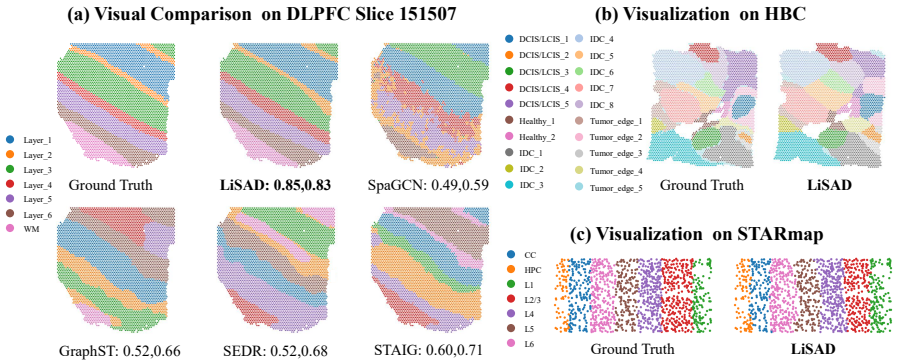

Fig. 2. Experimental visualization on three datasets. (a) On DLPFC slice 151507, LiSAD identifies seven laminar layers, achieving the highest ARI (0.85) and NMI (0.83). (b) On Human breast cancer, LiSAD captures complex tumor microenvironments accurately. (c) On STARmap, LiSAD delineates fine-grained anatomical regions, aligning closely with the ground truth.

there are substantial performance gains across all baselines relative to their unsupervised mode, validating the injection of minimal expert priors is a powerful strategy. Such results indicates that the performance gain in LiSAD is not only dependent on the additional supervision but also stems from the architectural advantages of our model.

The visual results in Fig. 2 further validate the efficacy of LiSAD. In the DLPFC slice 151507 (a), LiSAD successfully reconstructs the clear architecture with sharp and continuous boundaries, while baselines like SpaGCN and GraphST suffer from significant fragmented artifacts and misclassification. On HBC (b) and STARmap (c) datasets, LiSAD also identifies spatial domains that

Table 2. Ablation study of LiSAD modules on the DLPFC dataset.

Variant	Label-efficient	INR	SADTV	ARI	NMI
HAE				0.48	0.54
Label-efficient	✓			0.62	0.70
Label-efficient + INR	✓	✓		0.74	0.75
LiSAD (Full)	✓	✓	✓	**0.76**	**0.76**

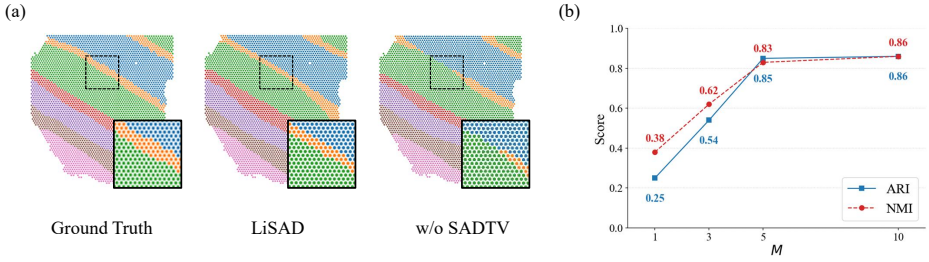

Fig. 3. Analysis of LiSAD on DLPFC slice 151507. (a) Visual comparison results are from left to right as the ground truth, LiSAD, and LiSAD without the SADTV. Dashed box region is zoomed in for more details. (b) Sensitivity analysis curve for the label number M.

are highly consistent with ground truths. Collectively, the visual improvements demonstrate the unique advantage of our proposed LiSAD model.

3.3 Ablation experiments

We conduct ablation experiments to quantify the contribution of each component. As shown in Table 2, the baseline model is a purely unsupervised hypergraph autoencoder (HAE) [2] using observed gene expressions X and coordinates P as input, which achieves an ARI of 0.48. Integrating few labels brings a substantial gain to 0.62 ARI, validating the effectiveness of label-efficiency strategy. Furthermore, the addition of the INR-enhanced continuous field significantly boosts the performance to 0.74 ARI, proving its effectiveness in filtering noise and modeling spatial continuity. Finally, the full LiSAD model with SADTV regularization achieves the highest ARI of 0.76. For a small number of boundary spots, this improvement is significant. Overall, all proposed components are essential and mutually beneficial.

To further investigate the impact of core components, we visualize the effect of SADTV and analyze the sensitivity to label density on slice 151507. As illustrated in the dashed boxes of Fig. 3(a), while the w/o variant struggles to resolve thin boundaries, LiSAD successfully identifies them through SADTV to amplify local variations. Furthermore, the sensitivity analysis in Fig. 3(b) analysis of the hyperparameter M. The ARI and NMI scores increase dramatically from $M = 1$

to 5 and reach a plateau thereafter, identifying $M = 5$ represents the optimal trade-off between cost and performance.

4 Conclusion

In this paper, we propose LiSAD, a label-efficient implicit model with spatially adaptive directional total variation for spatial domain identification. LiSAD transforms discrete ST data into a continuous spatial field via INRs. Meanwhile, a novel SADTV regularization is introduced to capture local directional variations, effectively preserving high-frequency spatial details at domain boundaries. Experimental results demonstrate that LiSAD significantly outperforms existing unsupervised methods with minimal labeling costs. Furthermore, the successful transfer of the label-efficient strategy validates its strong compatibility with interactive clinical workflows. Future work will extend LiSAD to 3D spatial transcriptomics analysis and resolution enhancement of ST data.

Acknowledgments. This work was supported by the National Natural Science Foundation of China [Grant No. 62572401 and No. 62322112], the Key Research and Development Program of Shaanxi [Program No. 2025SF-YBXM-424], and the Fundamental Research Funds for the Central Universities.

Disclosure of Interests. The authors have no competing interests to declare that are relevant to the content of this article.

References

1. Asp, M., Giacomello, S., Larsson, L., Wu, C., Fürth, D., Qian, X., Wärdell, E., Custodio, J., Reimegård, J., Salmén, F., et al.: A spatiotemporal organ-wide gene expression and cell atlas of the developing human heart. Cell **179**(7), 1647–1660 (2019)
2. Cai, Y., Zhang, Z., Cai, Z., Liu, X., Jiang, X.: Hypergraph-structured autoencoder for unsupervised and semisupervised classification of hyperspectral image. IEEE Geoscience and Remote Sensing Letters **19**, 1–5 (2021)
3. Chen, J., Zhou, M., Wu, W., Zhang, J., Li, Y., Li, D.: Stimage-1k4m: A histopathology image-gene expression dataset for spatial transcriptomics. Advances in Neural Information Processing Systems **37**, 35796–35823 (2024)
4. Dong, K., Zhang, S.: Deciphering spatial domains from spatially resolved transcriptomics with an adaptive graph attention auto-encoder. Nature Communications **13**(1), 1739 (2022)
5. Feng, Y., You, H., Zhang, Z., Ji, R., Gao, Y.: Hypergraph neural networks. In: Proceedings of the AAAI Conference on Artificial Intelligence. vol. 33, pp. 3558–3565 (2019)
6. Gao, Y., Feng, Y., Ji, S., Ji, R.: Hgnn+: General hypergraph neural networks. IEEE Transactions on Pattern Analysis and Machine Intelligence **45**(3), 3181–3199 (2022)
7. Guo, F., Shi, R., Zhou, J., Xu, J., Cui, H., Xuan, P., Feng, X., Wei, L., Su, R., Jin, Q.: Hrprotokd: A hierarchical and relational prototype based knowledge distillation framework for few-shot cancer molecular subtyping. IEEE Journal of Biomedical and Health Informatics pp. 1–12 (2025)

8. Hartigan, J.A., Wong, M.A.: Algorithm as 136: A k-means clustering algorithm. Journal of the Royal Statistical Society. Series C (Applied Statistics) **28**(1), 100–108 (1979)
9. Hu, J., Li, X., Coleman, K., Schroeder, A., Ma, N., Irwin, D.J., Lee, E.B., Shinohara, R.T., Li, M.: Spagcn: Integrating gene expression, spatial location and histology to identify spatial domains and spatially variable genes by graph convolutional network. Nature Methods **18**(11), 1342–1351 (2021)
10. Long, Y., Ang, K.S., Li, M., Chong, K.L.K., Sethi, R., Zhong, C., Xu, H., Ong, Z., Sachaphibulkij, K., Chen, A., et al.: Spatially informed clustering, integration, and deconvolution of spatial transcriptomics with graphst. Nature Communications **14**(1), 1155 (2023)
11. Luo, Y., Zhao, X., Li, Z., Ng, M.K., Meng, D.: Low-rank tensor function representation for multi-dimensional data recovery. IEEE Transactions on Pattern Analysis and Machine Intelligence **46**(5), 3351–3369 (2023)
12. Luo, Y., Zhao, X., Ye, K., Meng, D.: Neurtv: total variation on the neural domain. SIAM Journal on Imaging Sciences **18**(2), 1101–1140 (2025)
13. Luo, Y., Zhao, X., Ye, K., Meng, D.: Stinr: Deciphering spatial transcriptomics via implicit neural representation. In: Proceedings of the IEEE/CVF Conference on Computer Vision and Pattern Recognition. pp. 25930–25939 (2025)
14. Maynard, K.R., Collado-Torres, L., Weber, L.M., Uytingco, C., Barry, B.K., Williams, S.R., Catallini, J.L., Tran, M.N., Besich, Z., Tippani, M., et al.: Transcriptome-scale spatial gene expression in the human dorsolateral prefrontal cortex. Nature Neuroscience **24**(3), 425–436 (2021)
15. Pham, D., Tan, X., Balderson, B., Xu, J., Grice, L.F., Yoon, S., Willis, E.F., Tran, M., Lam, P.Y., Raghubar, A., et al.: Robust mapping of spatiotemporal trajectories and cell–cell interactions in healthy and diseased tissues. Nature Communications **14**(1), 7739 (2023)
16. Qu, H., Wu, P., Huang, Q., Yi, J., Yan, Z., Li, K., Riedlinger, G.M., De, S., Zhang, S., Metaxas, D.N.: Weakly supervised deep nuclei segmentation using partial points annotation in histopathology images. IEEE Transactions on Medical Imaging **39**(11), 3655–3666 (2020)
17. Rao, N., Clark, S., Habern, O.: Bridging genomics and tissue pathology: 10x genomics explores new frontiers with the visium spatial gene expression solution. Genetic Engineering & Biotechnology News **40**(2), 50–51 (2020)
18. Singhal, V., Chou, N., Lee, J., Yue, Y., Liu, J., Chock, W.K., Lin, L., Chang, Y.C., Teo, E.M.L., Aow, J., et al.: Banksy unifies cell typing and tissue domain segmentation for scalable spatial omics data analysis. Nature Genetics **56**(3), 431–441 (2024)
19. Sitzmann, V., Martel, J., Bergman, A., Lindell, D., Wetzstein, G.: Implicit neural representations with periodic activation functions. Advances in Neural Information Processing Systems **33**, 7462–7473 (2020)
20. Ståhl, P.L., Salm'en, F., Vickovic, S., Lundmark, A., Navarro, J.F., Magnusson, J., Giacomello, S., Asp, M., Westholm, J.O., Huss, M., et al.: Visualization and analysis of gene expression in tissue sections by spatial transcriptomics. Science **353**(6294), 78–82 (2016)
21. Traag, V.A., Waltman, L., Van Eck, N.J.: From louvain to leiden: guaranteeing well-connected communities. Scientific reports **9**(1), 5233 (2019)
22. Wang, X., Allen, W.E., Wright, M.A., Sylwestrak, E.L., Samusik, N., Vesuna, S., Evans, K., Liu, C., Ramakrishnan, C., Liu, J., et al.: Three-dimensional intact-tissue sequencing of single-cell transcriptional states. Science **361**(6400), eaat5691 (2018)

23. Xu, C., Jin, X., Wei, S., Wang, P., Luo, M., Xu, Z., Yang, W., Cai, Y., Xiao, L., Lin, X., et al.: Deepst: identifying spatial domains in spatial transcriptomics by deep learning. Nucleic Acids Research **50**(22), e131–e131 (2022)
24. Xu, H., Fu, H., Long, Y., Ang, K.S., Sethi, R., Chong, K., Li, M., Uddamvathanak, R., Lee, H.K., Ling, J., et al.: Unsupervised spatially embedded deep representation of spatial transcriptomics. Genome Medicine **16**(1), 12 (2024)
25. Xuan, P., Yang, X., Chen, S., Cui, H., Xu, Z., Jin, Q., Zhang, T.: Topology-enhanced hypergraph learning and adaptive multi-graph transformer for prediction of drug-related side effects. Expert Systems with Applications **320**, 132150 (2026)
26. Yang, Y., Cui, Y., Zeng, X., Zhang, Y., Loza, M., Park, S.J., Nakai, K.: Staig: Spatial transcriptomics analysis via image-aided graph contrastive learning for domain exploration and alignment-free integration. Nature Communications **16**(1), 1067 (2025)
27. Zhang, L., Liang, S., Wan, L.: A multi-view graph contrastive learning framework for deciphering spatially resolved transcriptomics data. Briefings in Bioinformatics **25**(4), bbae255 (2024)
28. Zhao, E., Stone, M.R., Ren, X., Guenthoer, J., Smythe, K.S., Pulliam, T., Williams, S.R., Uytingco, C.R., Taylor, S.E., Nghiem, P., et al.: Spatial transcriptomics at subspot resolution with bayesspace. Nature Biotechnology **39**(11), 1375–1384 (2021)